Biomaterials and Biosystems 16 (2024) 100103

Contents lists available at ScienceDirect

Biomaterials and Biosystems

journal homepage: www.elsevier.com/locate/bbiosy

Enhanced osteogenic potential of spider silk fibroin-based composite scaffolds incorporating carboxymethyl cellulose for bone tissue engineering

Woong Jin Lee [a,1], Kyoungjoo Cho [b,1], Dayoon Lee [a], Seungmin Lee [a,c], Hyojae Jeon [a], Aaron Youngjae Kim [a,d], Gyung Whan Kim [a,*]

[a] Department of Neurology, College of Medicine, Yonsei University, Seoul, South Korea
[b] Department of Life Science, Kyonggi University, Suwon, South Korea
[c] College of Medicine, Ewha Womans University, Seoul, South Korea
[d] Weill Cornell Medicine-Qatar, Doha, Qatar

ARTICLE INFO

Keywords:
Silks
Scaffold
Carboxymethyl cellulose (CMC)
Osteocyte
Regenerative medicine

ABSTRACT

This study aimed to investigate the characteristics of composite scaffolds that combine fibroin derived from spider silk and carboxymethyl cellulose (CMC) in the field of bone tissue engineering. Fibroin, obtained from spider silk, serves as a valuable biomaterial and constitutes the primary component of fibrous protein-based spider silk threads. To enhance the binding efficiency in bone formation after scaffold implantation, CMC was integrated into fibroin, aiming to improve the injectability properties of the scaffold in bone substitutes. For bone marrow mesenchymal stem cell (BMSC) tissue engineering, BMSCs isolated from mice were seeded onto the scaffold, and the rate of cell proliferation was assessed. The composite scaffold, with the addition of CMC to fibroin, exhibited superior characteristics compared to scaffolds containing only silks, including porous morphology, porosity, surface wettability, water absorption, and thermal properties. Alkaline phosphatase activity in BMSCs was significantly higher in the CMC-containing scaffold compared to the silk-only scaffold, and the CMC-containing scaffold demonstrated increased expression of osteocyte marker genes and proteins. In conclusion, the biocompatibility and hydrophilicity of CMC-containing scaffolds play essential roles in the growth and proliferation of osteocytes. Furthermore, the CMC-containing scaffold design proposed in this study is expected to have a substantial impact on promoting ossification of BMSCs.

1. Introduction

Scaffolds are a crucial component in tissue engineering, providing a supportive structure for cell growth and tissue regeneration. Rather than serving merely as passive carriers for cells, scaffolds actively support cellular functions such as adhesion, migration, proliferation, and differentiation. These properties are essential for creating tissues that mimic natural structures and promote effective healing. An ideal scaffold must support these cellular functions while maintaining structural integrity and facilitating the exchange of oxygen and nutrients to the cells. Moreover, scaffolds should interact with biochemical agents, such as growth factors and extracellular matrix components, to encourage tissue regeneration [1].

Scaffolds are typically made from a variety of materials, including natural and synthetic polymers, ceramics, and metals such as titanium, which are chosen based on their biocompatibility, mechanical properties, and the specific needs of the tissue being regenerated. Among these, natural polymers like collagen, hyaluronic acid, and fibrin are particularly promising due to their ability to mimic the extracellular matrix (ECM), which is essential for cell survival and function. However, challenges remain, especially in processing natural polymers to achieve the desired mechanical strength and ease of handling in clinical settings. Additionally, some natural polymers may lack the necessary mechanical properties for certain applications, such as load-bearing tissues [2–4].

Fibroin, a protein derived from silkworms and spiders, has attracted considerable attention in scaffold development due to its mechanical strength, biocompatibility, and biodegradability. The fibroin obtained from silkworms is widely used in tissue engineering, but spider silk, with

* Corresponding author.
E-mail addresses: osang0616@yuhs.ac (W.J. Lee), kcho0611@kgu.ac.kr (K. Cho), smlee0458@ewhain.net (S. Lee), Yok2019@qatar-med.cornell.edu (A.Y. Kim), gyungkim@yuhs.ac (G.W. Kim).
[1] The authors equally contributed to this article.

https://doi.org/10.1016/j.bbiosy.2024.100103
Received 5 July 2024; Received in revised form 17 November 2024; Accepted 18 November 2024
Available online 19 November 2024

its unique mechanical properties such as high tensile strength and elasticity, is emerging as a preferred material for scaffolds in specific applications like tendon and ligament regeneration. Spider silk's mechanical strength is attributed to its high strain tolerance and excellent fatigue resistance, which are vital for scaffolds that need to provide support and flexibility, such as those used in bone tissue engineering [5].

In this context, natural polymers such as carboxymethyl cellulose (CMC) are increasingly being explored for their role in scaffold fabrication. CMC, derived from cellulose through ether derivation, possesses excellent water solubility and can improve the injectability of scaffold materials, making it ideal for minimally invasive procedures. When combined with silk fibroin, CMC enhances the properties of the resulting scaffold, particularly in promoting bone formation [6–8]. In our study, CMC was incorporated into silk-based scaffolds, and the physical properties of the resulting polymer were thoroughly analyzed through mechanical, chemical, and biological assessments. The CMC-containing scaffolds demonstrated enhanced performance in facilitating ossification and differentiation of bone marrow-derived stem cells (BMSCs), indicating their potential in regenerative medicine [9–11].

The mechanical properties of spider silk and the addition of CMC contribute to scaffolds that can support both the structural and functional demands of bone regeneration. While the high tensile strength of spider silk plays a critical role in providing the necessary mechanical support, the CMC component enhances the scaffold's biocompatibility and its ability to promote cell differentiation. The results of our study underscore the significant potential of CMC-containing silk scaffolds for applications in bone tissue engineering, particularly in accelerating ossification and supporting the regeneration of complex tissues [12]. These findings suggest that the synergy between natural polymers like fibroin and CMC could pave the way for more effective and versatile scaffolds in regenerative medicine. [13]

In conclusion, scaffolds made from natural polymers like silk fibroin and CMC offer promising strategies for tissue engineering. The incorporation of CMC into silk scaffolds not only improves their mechanical properties but also facilitates the differentiation of stem cells into bone tissue, making them valuable for regenerative applications. Future research should focus on optimizing the processing methods for these materials to enhance their properties further and broaden their clinical applications.

2. Materials and methods

2.1. Fabrication of CMC porous scaffold containing silks

A schematic of silks/CMC/gelatin scaffold production is shown in Fig. 1. We attempted to determine conditions that would provide an optimal environment for cell growth by adding CMC, gelatin, and crosslinking agents to silks and varying the concentration of each component. Silks were collected directly from spiders living in South Korea. A silk solution was prepared by dissolving 10 g of silks in 9.3 M LiBr solution at 70 °C for 2 h 30 min and dialyzed on a cellulose membrane [14–16]. Tertiary distilled water was replaced every 6 h for three days to eliminate LiBr. The supernatant was obtained after centrifugation at 9000 rpm for 20 min at 4 °C. Protein concentration was measured using the Bradford standard assay. A total of 50 % of the silk solution purified via the aforementioned method was placed into a 24-well plate, and 0 %, 10 %, 20 %, and 50 % of the CMC solution was dispensed, respectively. Then, to induce the formation of a porous sponge, a scaffold was prepared in which 4 % gelatin solution and 2.5 % glutaraldehyde mixed aqueous solution (used as a cross-linking agent) were added to the aforementioned solution. The scaffold was stored at 4 °C and −20 °C for 8 h, cooled at −80 °C for 24 h, then lyophilized by freeze-drying at −80 °C for 48 h Subsequently, cross-linking in the scaffold was inhibited using 100 % glycine, followed by washing the scaffold five times with tertiary distilled water to remove glycine solution. After drying in a vacuum oven at 25 °C for at least one week to remove the residual solvent, ethylene oxide (EO) sterilization was performed. The scaffolds were used for cell culture experiments after sterilization [17,18].

2.2. Surface observation and porosity analysis of scaffolds

To evaluate the macroscopic features of each scaffold, including Silks

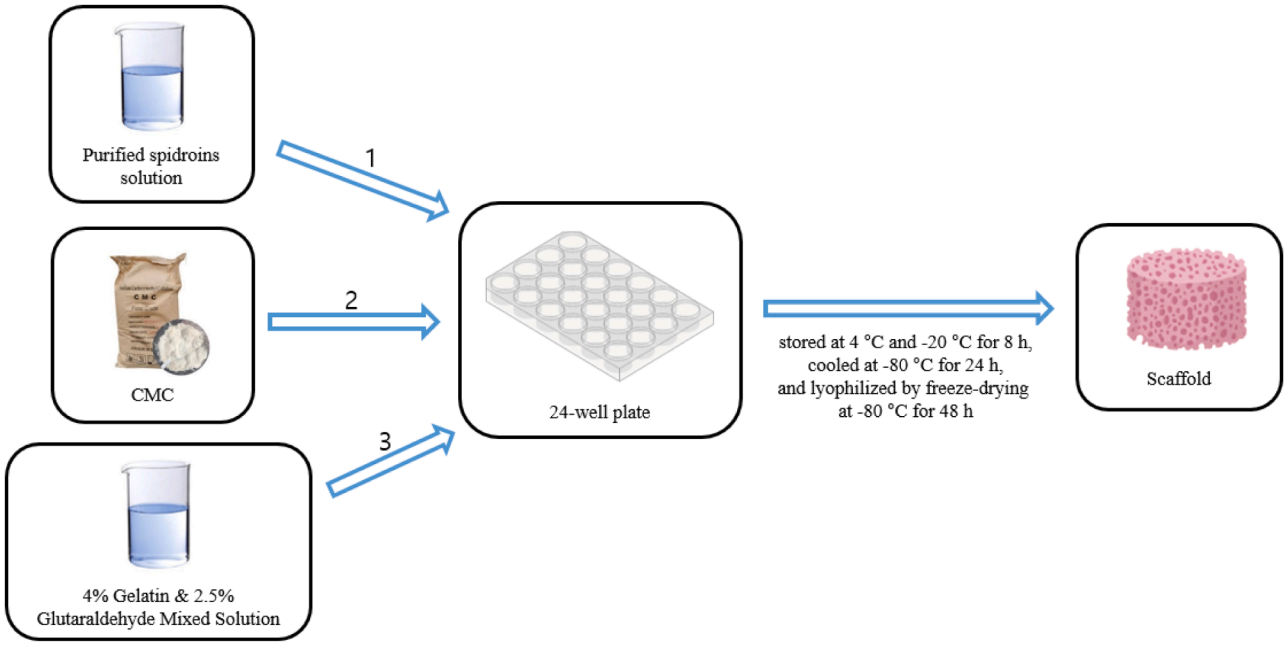

Fig. 1. Fabrication of CMC porous scaffolds containing silks. Schematic diagram of the fabrication process of Silks and Silks + CMC (50 %) composite scaffolds obtained by freeze-drying method.

An SEM image of the prepared porous Silks and Silks + CMC (50 %) composite scaffolds is shown in Fig. 2. The porous shapes of the inner and side surfaces of the support appeared to be similar to those of the salt particles. No significant morphological difference was observed between the support containing silks and the porous morphology without silks (Fig. 2).

and Silks + CMC (50 %) composite scaffolds, we captured high-resolution images of the scaffold samples. The silks solution was cast in a standardized mold and subjected to freeze-drying to produce a porous structure. Photographs of each scaffold were taken under controlled lighting conditions to capture visible morphological differences. Additionally, scaffold thickness and pore uniformity were noted to assess structural consistency across samples.

The surface and inner porous morphologies of the porous support prepared via the aforementioned method were observed using a scanning electron microscope (SEM, JSM-6400, JEOL, Japan). The shape of the pores was confirmed using a photograph captured by imaging the scaffold cut with a scalpel into a size of 5 mm × 5 mm × 1 mm and coated using plasma sputtering. The pore size, distribution, average diameter, and porosity of the prepared porous support were measured using a mercury porosimeter [19].

2.3. X-ray photoelectron spectroscopy (XPS) analysis

X-ray photoelectron spectroscopy (XPS) is used for analyzing photoelectrons generated by irradiating X-rays on the surface of a sample. When X-rays are projected onto the surface of a sample, electrons in the atoms receive energy and are ejected. If the kinetic energy of an electron is measured, and the unique work function of each element is known, the binding energy can be measured. Using the binding energy measured in this manner, it is possible to determine the type of material present on the surface of the sample. Such surface analysis can identify elements, chemical bonding states, and energy levels of surfaces and interfaces from the surface to a depth of approximately 20 Å for hard materials such as metals and approximately 100 Å for organic or polymeric materials. For the XPS analysis, Thermo VG Scientific K-alpha (Waltham, MA, USA) was used [20].

2.4. Structural analysis using H-NMR

Nuclear magnetic resonance (NMR) spectroscopy is used for measuring the spin of atoms constituting a sample. The structure of the scaffold was examined via nuclear magnetic resonance. In this study, the spin of hydrogen was investigated and confirmed using a spectrometer. Each sample (500 μL) was prepared to obtain a concentration of 10 mg/mL, and D2O (Cambridge Isotope Laboratories, Inc.) was used as the solvent [21].

2.5. Hydrophilicity measurement

To examine the hydrophilic effect of the porous support according to the silks content, trypan blue dye was dropped onto the support and the degree of absorption over time was observed. The effect of dye penetration was analyzed 20, 40, 60, 80, and 100 min after dropping the trypan blue dye by measuring the contact angle [22].

2.6. Water absorption rate measurement

To measure the water absorption capacity of the prepared scaffolds, the following experiment was performed. First, the initial weight of the scaffold was measured and left at room temperature in 10 mL of water for 3, 5, 7, and 10 days. After eliminating moisture from the surface of the scaffold that had absorbed water, the weight was measured, and the water absorption rate was measured by substituting it in the water uptake [23]. All experiments were performed three times under the same conditions.

2.7. Isolation and culture of BMSCs

Primary BMSCs were isolated and cultured using a previously reported method [24]. After making an incision on the thigh of a Fischer rat (female, three-week-old), 2–3 mL of bone marrow was collected using an 18-gauge needle. The collected bone marrow was diluted twice with the culture solution to 50 % Percoll (Sigma Aldrich, MJ, USA) and then slowly dropped into the gradual gradient solution to prevent mixing with the Percoll layer. The solution was centrifuged at 280 g for 25 min to separate layers of red blood cells, Percoll, plasma, and other cells. Using a micropipette, only the cell layer was separated, diluted again with the culture medium, and centrifuged at 150 g for 10 min. Subsequently, the cells were washed twice or three times with the culture medium. The supernatant was removed, and the separated cells were treated with 10 % fetal bovine serum (FBS, Gibco, MA, USA) and antibiotics (100 unit/ml penicillin and 100 μg/mL streptomycin, Gibco). The cells were cultured in Dulbecco's modified Eagle's medium (DMEM; low glucose, Gibco, USA) in a culture flask to obtain a density of 2 × 104 cells/cm^2. The cells were cultured once every three days and sub-cultured once every seven days [25]. The isolated BMSCs were verified through von Kossa staining at DIV 0, 6, 9, and 15.

2.8. MTT assay

3-(4,5-dimethythiazol-2-yl)−2,5-diphenyl-tetrazolium bromide (MTT, Sigma-Aldrich, USA) was used to evaluate the cytotoxicity of the prepared scaffolds. BMSCs were used for cytotoxicity evaluation. The cells were injected into a 96-well plate with the prepared scaffold to obtain a density of 1.3 × 105 cells/mL, followed by culturing the cells in an incubator for 24 h After 24 h, the treated supernatant was removed, 200 μg/mL of MTT solution added, and incubated for 1 h and 30 min at 37 °C in the dark (the light was blocked). Subsequently, the MTT solution was removed, and the cells were washed twice with PBS. After washing, 200 μL of DMSO (Sigma-Aldrich, USA) was injected. The reaction was performed for 30 min. Cytotoxicity was evaluated by measuring the absorbance at a wavelength of 570 nm using a microplate reader (Thermo Fisher Scientific, MA, USA) [26].

2.9. Alkaline phosphatase assay

After inoculation of BMSCs on Silks and Silks + CMC (50 %) composite scaffolds, the activity of alkaline phosphatase assay (ALP) specifically expressed in osteoblasts was measured using the TRACP & ALP kit (Takara Bio Inc., Japan) to confirm differentiation into osteocytes according to CMC content. After removing the culture solution on days 1, 3, 7, and 14 and washing the cultured sample with physiological saline, 500 μL of the extract solution was mixed and stirred for 1 h After centrifuging the mixture at 13,000 rpm for 10 min, the supernatant was collected, mixed with the substrate solution and the mixture in a 1:1 ratio, and incubated at 37 °C for 1 h Then, 0.9 N NaOH was added to stop the enzymatic reaction, and the absorbance was measured at 405 nm by adding 100 μL of each reaction solution [27].

2.10. Immunofluorescence staining

Immunofluorescence staining was performed on cultured mesenchymal stem cells. To increase cell permeability, 0.2 % Triton X-100 was added and reacted at room temperature for 15 min. Normal goat serum was then used to suppress non-specific reactions at 37 °C for 1 hour, and primary antibodies were diluted to an appropriate ratio and incubated at 37 °C for 1 h After incubation, the secondary antibodies were added following three 5-min washes with PBS. The secondary antibody was prepared by diluting FITC (Fluorecein isothiocynate)-conjugated goat antimouse IgG (Zymed, San Francisco, USA, 1:50) and TRITC (tetramethyrhodamin isothiocynate)-conjugated IgG (Zymed, San Fran-cisco, USA, 1:30), and reacted at 37 °C for 1 h After three additional washes with PBS, Hoechst 33,258 (Sigma, St. Louis, USA, 1 μg/mL) was used for counterstaining at room temperature for 15 min, followed by sealing with a Fluorescence medium and observation under a fluorescence microscope.

2.11. Alizarin red staining

Calcium mineralization was determined by Alizarin Red S staining. BMSC cells were then incubated in the osteogenic differentiation medium. During the incubation, the media was changed every 2 days. After that, the BMSC cells were fixed with 10 % formaldehyde and stained with Alizarin Red S in deionized water (pH = 4.1–4.3) for 1 h at 25 ℃. After removing the Alizarin Red S by aspiration, the BMSC cells were washed three times with deionized water. For quantification, Alizarine RedS-dyed cells were destained with cetylpyridinium chloride, then the absorbance value was monitored at 450 nm using a microplate reader.

2.12. Western blotting analysis

After extraction with RIPA buffer, the protein was quantitatively analyzed using the bicinchoninic acid (BCA) assay. Based on this, 100 μg of protein was used for electrophoresis. Each protein sample mixed with a pre-stained protein marker (Bio-Rad, CA, USA) and loading buffer was denatured at 95 °C for 5 min, electrophoresed on 12.5 % SDS-PAGE gel, and then transferred to a nitrocellulose membrane (Bio-Rad, USA). After blocking the nitrocellulose membrane in a membrane blocking solution (Zymed, CA, USA) for 1 h, each antibody was diluted in a 400:1 ratio in the blocking solution; the reaction was carried out for 90 min. The reaction with the secondary antibody (HRP-conjugated anti-mouse IgG, Santa Cruz Biotechnology, TX, USA) was performed for 1 h Detection was performed using an ECL chemiluminescence detection kit (Amersham, NJ, USA) [28].

2.13. Fourier-Transform infrared (FTIR) spectroscopy analysis

Fourier-Transform Infrared (FTIR) Spectroscopy was utilized to analyze the chemical composition and functional groups of the scaffold samples. FTIR operates by passing infrared light through the sample, where molecular bonds absorb specific wavelengths corresponding to their vibrational frequencies. These absorbed wavelengths are detected and converted into a spectrum that represents the sample's molecular fingerprint. Key functional groups in silks and carboxymethyl cellulose (CMC) are identifiable by characteristic absorption peaks, such as the Amide I (1640 cm^{-1}) and Amide II (1515 cm^{-1}) bands for proteins. The FTIR spectra for each scaffold were recorded using a PerkinElmer Spectrum Two FTIR Spectrometer (Waltham, MA, USA), scanning from 4000 to 400 cm^{-1}, with an average of 32 scans per measurement to ensure signal accuracy. This analysis helped to confirm the chemical interactions and composition of the Silks + CMC (50 %) composite structure in the scaffold samples.

2.14. Fluorescence-Activated cell sorting (FACS) analysis

Fluorescence-Activated Cell Sorting (FACS) was employed to analyze cell populations by detecting fluorescently labeled surface markers, allowing for quantitative assessment of specific cellular phenotypes. For FACS analysis, cells were harvested and washed twice with phosphate-buffered saline (PBS) to remove any residual media. Following this, cells were resuspended at a concentration of 1 × 10^6 cells/mL in PBS supplemented with 1 % bovine serum albumin (BSA) to prevent nonspecific binding. To label target antigens, cells were incubated with fluorophore-conjugated antibodies (e.g., anti-CD90-FITC, anti-CD105-PE) at optimal dilutions (e.g., 1:100) for 30 min at 4 °C in the dark. After incubation, the cells were washed twice with PBS containing 1 % BSA to remove unbound antibodies. Finally, the stained cells were resuspended in 500 μL of PBS and filtered through a 40 μm cell strainer to ensure single-cell suspension. For analysis, the prepared samples were run on a BD FACSAria III (Becton Dickinson, Franklin Lakes, NJ, USA), and data were processed using BD FACSDiva software. Gates were set based on unstained and isotype controls to accurately quantify positive populations, ensuring reliable identification of cell subsets.

3. Results

3.1. Fabrication of CMC porous scaffold and analysis of the scaffold surface

Macroscopic Features of the Silks and Silks + CMC (50 %) composite scaffolds

The macroscopic images of the scaffolds revealed clear distinctions in physical structure between the Silks and Silks + CMC (50 %) composite scaffolds. As shown in Supplementary Figure 1, the Silks scaffold had a dense, smooth surface with minimal visible porosity. In contrast, the Silks + CMC (50 %) composite scaffolds displayed a progressively porous and sponge-like structure, with increased pore size and distribution correlating with the higher CMC concentrations (10 %, 20 %, and 50 %). The scaffolds containing 50 % CMC exhibited the highest porosity and sponginess, potentially enhancing hydrophilicity and cellular attachment. These macroscopic characteristics suggest that CMC addition effectively modulates the scaffold's structural properties, creating a more favorable environment for cell proliferation and differentiation.

Porous support containing silks was prepared using the solvent-casting freeze drying method. The external shape was identical to that of the silicone mold, and no shrinkage, swelling, holes with irregular sizes, or other defects were observed (Fig. 2).

3.2. Surface and structural analysis of silks and silks + CMC (50 %) composite scaffolds via XPS and H-NMR

To fully elucidate the functional groups and interactions on the CMC surface, we performed XPS measurements of Silks and Silks + CMC (50 %) composite scaffolds (Fig. 3A).

The broad-scan spectrum showed three sharp peaks corresponding to silks (C 1 s, O 1 s, and N 1 s) consisting of the previous reports [29]. This XPS spectrum was consistent with the chemical structure of polysaccharide CMC; three peaks (C1 s, N1 s, and O1 s) corresponding to Silks/CMC were observed. The presence of C1 s, O1 s, and N1 s peaks at each eV demonstrated the successful integration of CMC into silks. The XPS spectra corresponding to the Silks/CMC membrane surface in the C1 s, O1 s, and N1 s regions showed the presence of an organic polysaccharide shell. As expected, the spectrum primarily demonstrated signals corresponding to carbon (C1 s) and oxygen (O1 s).

The structure of each compound was confirmed using the H—NMR spectrum, and the degree of substitution of the catechol group was evaluated by comparing the peak areas corresponding to the proton of the catechol group (3H, 6.75–6.88 ppm) and the proton of the acetyl group (3H, 2.1–2.25 ppm) (Fig. 3B). A typical characteristic peak was detected in the silks NMR spectrum (Fig. 3B, left). On the other hand, the H—NMR spectrum of Silks/CMC presented that a catechol group was introduced into silks (Fig. 3B, right). In the synthesized Silks/CMC, a peak of the catechol group was observed near 7 ppm, and Silks/CMC was well synthesized, as demonstrated by this new peak corresponding to the catechol group. The change in the substitution degree of the catechol group in Silks/CMC was observed according to the amount of CMC in an aqueous solution of pH 5.5. As the amount of CMC increased during the reaction, the degree of substitution increased. However, no significant change was observed at an input amount of 1 g or more. In addition, the substitution degree of the catechol group was changed when increasing the pH from 5.5 to 7.5 by fixing the input amount of CMC to 1 g. The amount of CMC (1 g) and pH (6.5) were fixed as the reaction conditions for Silks/CMC with a maximum degree of substitution of 38.6 % (Fig. 3B).

3.3. Properties of the silks/CMC

The mercury porosimetry analysis showed that there is a minor difference in porosity distribution when the content of silks was approximately 50 % (Fig. 2B). However, analysis of the porosity and median

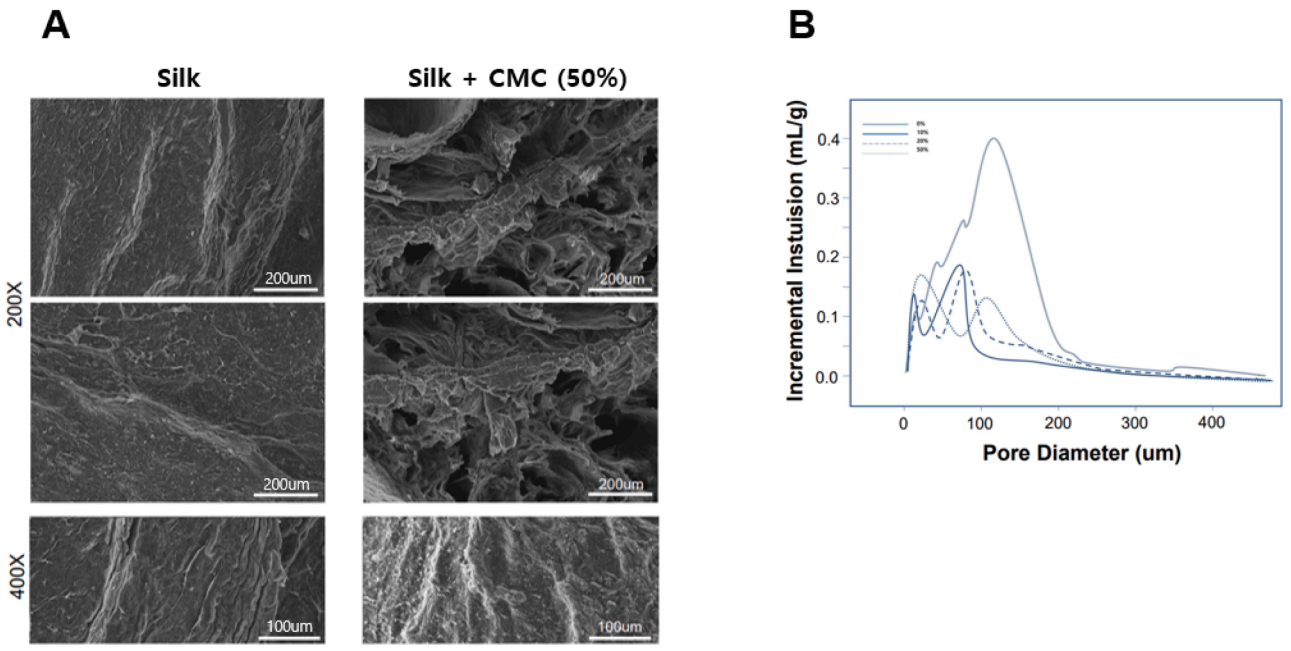

Fig. 2. (A) SEM micrographs of Silks and Silks + CMC (50 %) composite scaffolds developed via freeze-drying. (B) Properties of the CMC-containing scaffold. (A) Mercury porosimetry analysis displays the pore size distributions of Silks and Silks + CMC composite scaffolds(Silks/CMC). 0 %, silks; 10 %, Silks/CMC (10 wt %); 20 %, Silks/CMC (20 wt %); and 50 %, Silks/CMC (50 wt %).

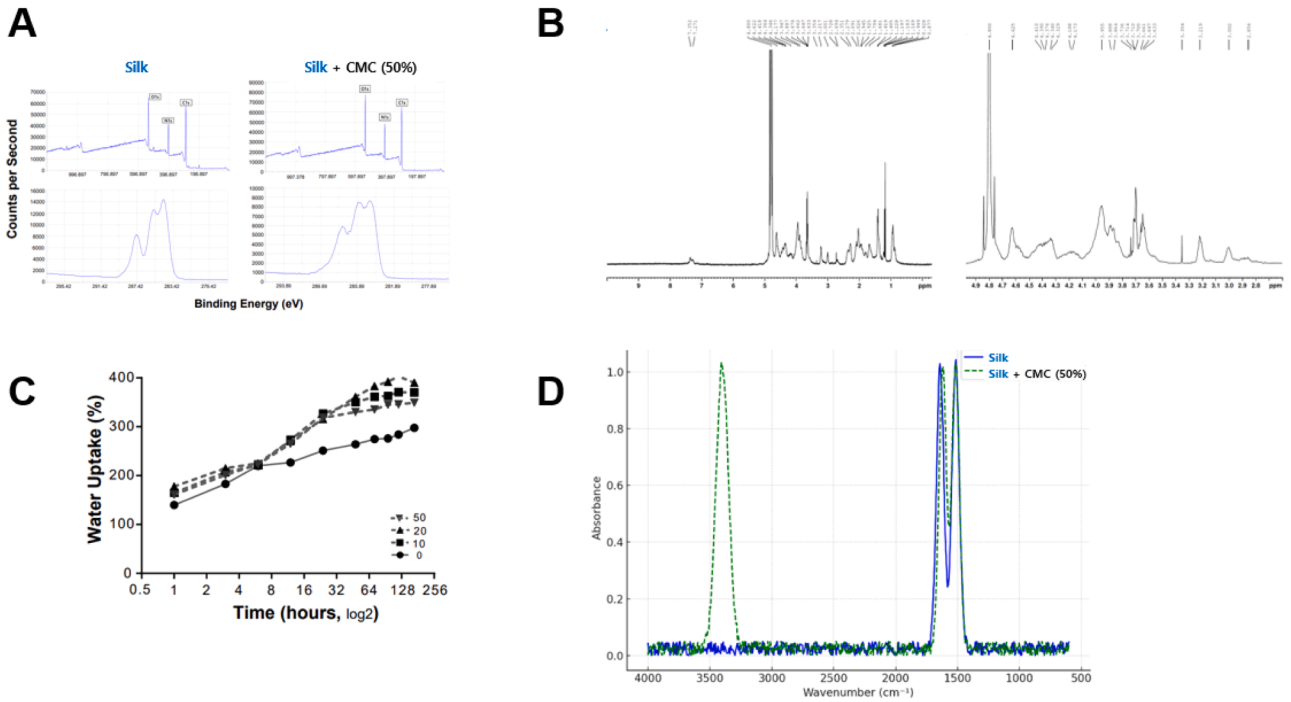

Fig. 3. Mechanical analysis of the CMC. (A) The XPS survey spectra of the silks scaffold before and after the addition of CMC in X-ray photoelectron spectroscopy (XPS). (B) H NMR spectra were measured in Silks (left) and Silks + CMC (50 %) composite scaffolds (right). (C) Absorption rate was evaluated as water-uptake ability of the scaffold with respect to CMC concentration. 0 %, Silks; 10 %, Silks/CMC (10 wt %); 20 %, Silks/CMC (20 wt %); and 50 %, Silks/CMC (50 wt %). (D) FTIR Spectra of Silks and Silks + CMC (50 %) composite scaffolds with Reduced Peaks. The FTIR spectra illustrate characteristic absorption bands for Silks (blue) and Silks + CMC (50 %) composite (green, dashed) scaffolds. Key peaks observed around 1640 cm^{-1} and 1515 cm^{-1} correspond to Amide I and Amide II bands, indicative of protein structure. For the Silks + CMC (50 %) composite scaffolds, an additional peak at approximately 3400 cm^{-1} reflects CMC incorporation, enhancing scaffold hydrophilicity. Peaks have been simplified to approximately ten main signals to match established literature data.

pore size showed no significant difference with respect to the content of silks. When the silks content was significantly increased, a small difference in pore size was observed. As the silks content is increased, the protein is expected to block the periphery of the pores slightly. However, the concentration is within a range that does not significantly affect the adhesion and growth of cells. A porosity of 65 % or more was observed in all samples, thereby confirming that a support with a constant size and porosity was prepared even after the addition of silks (Fig. 2B),

consistent with a previous report [30].

The hydrophilic effect observed that the CMC-containing scaffold had a moisture content of approximately 430 %, and the silks-only scaffold without CMC had a maximum moisture content of 320 % (Fig. 3C). The initial moisture content was high in 50 wt % Silks /CMC scaffold. However, after 48 h, the moisture content was lower than that in the 10 or 20 wt % Silks/CMC scaffold. Hence, 50 wt % Silks scaffold contained two to four-fold higher silk content than other samples of the same volume and showed a lower absorption rate than 10 or 20 wt % Silks/scaffold after a certain period due to its high density. The higher water content of the CMC-containing scaffold can be attributed to hydrophilic amino acids, such as glutamic acid, arginine, and cysteine, which are major components of silks [31].

3.4. Identification of BMSCs under the silks and silks + CMC (50 %) composite scaffolds

BMSCs were isolated from the femur and cultured for approximately three passages. Cellular morphology was analyzed after three weeks to assess mesenchymal stem cell (MSC) development. Histological staining of MSC to differentiate into bone. The von Kossa-stained MSCs were visualized in black by silver nitrate. Von Kossa staining confirmed the presence of MSCs derived from rat bone marrow (Fig. 4A).

3.5. The beneficial effect of CMC-containing scaffold on osteogenic differentiation

The growth of BMSCs in scaffolds with various CMC contents was compared using MTT analysis. Cytotoxicity was not detected in CMC-containing scaffold or the Silks scaffold alone (Fig. 5A). Particularly, in 10 or 20 wt % Silks/CMC scaffold, the viability of BMSCs showed a slight increase. ALP activity, an extracellular enzyme produced by osteoblasts and an indicator of bone formation, was assessed in BMSCs that seeded on the prepared silk/CMC scaffold. The activity of ALP, an early marker of osteo-differentiation, was starting to rise in scaffolds containing CMC on the first day (data not shown). The final ALP activity at day 14 had increased higher in the CMC-containing scaffold than that in the Silks-only scaffold (Fig. 5B). Since the CMC-containing scaffold demonstrated differentiation into osteocytes, the ALP activity corresponding to differentiation into osteoblasts may increase, as previously reported. Furthermore, to confirm the phenotype of BMSCs on Silks/CMC scaffolds, proteins related to osteoblasts were analyzed by western

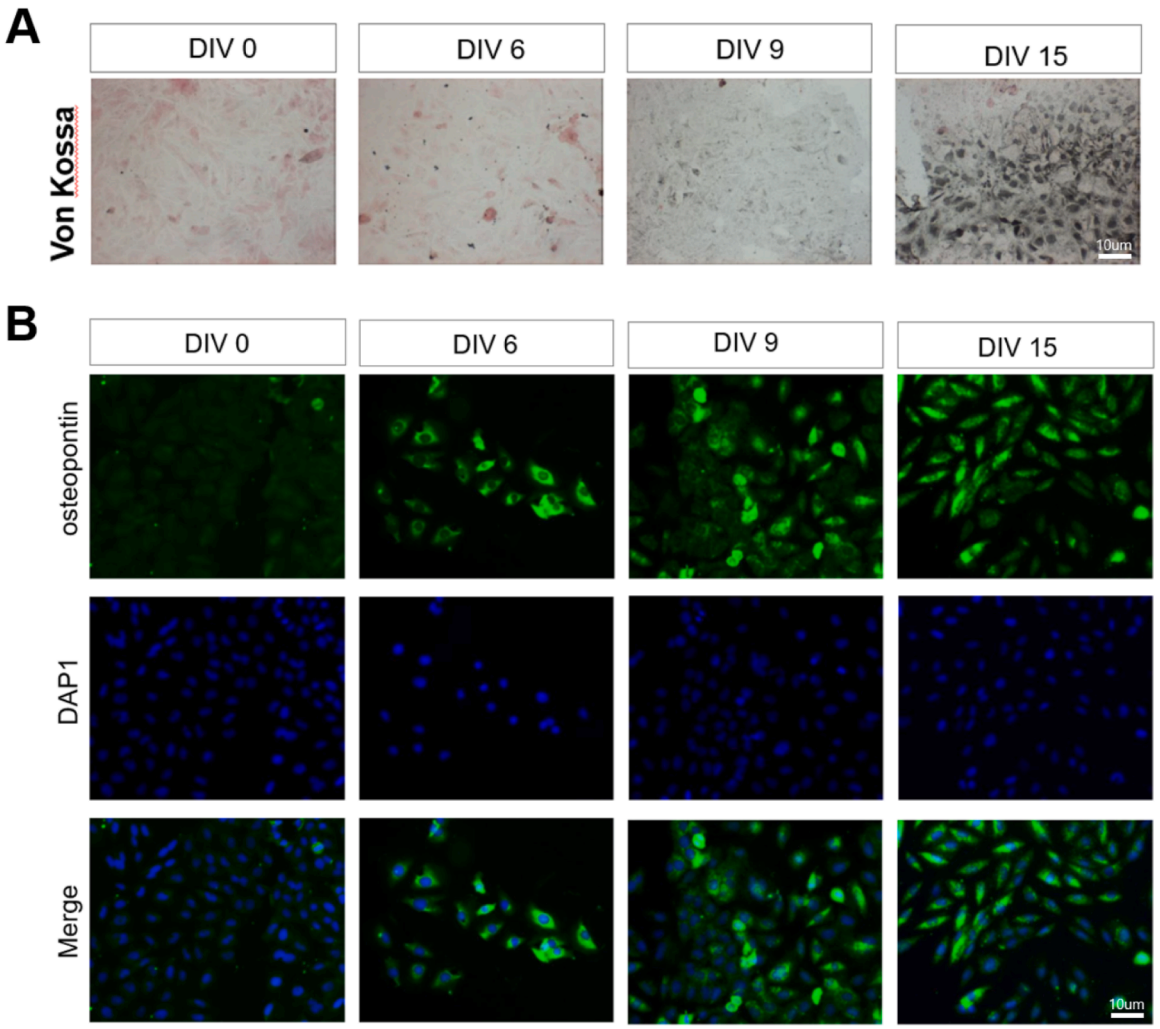

Fig. 4. Identification of BMSCs. (A) Histological staining of MSC to differentiate into bone. The von Kossa stained cells (MSCs) were visualized in black by silver nitrate. (B) Further analysis of MSC was shown in Immunofluorescence staining of osteopontin. Immunofluorescence was visualized using FITC (green) and the nuclei by DAPI (blue). The morphology of which was primarily spindle-shaped and polygonal.
On the day of 12 after culture, the mesenchymal stem cells exhibited highly expression of each bone-related protein, osteopontin (Fig. 4B). The osteogenic differentiation effect of the CMC-containing scaffold on BMSCs was evaluated through osteopontin immunocytochemistry of osteopontin, showing changes over time (Fig. 4B) Fig. 2.

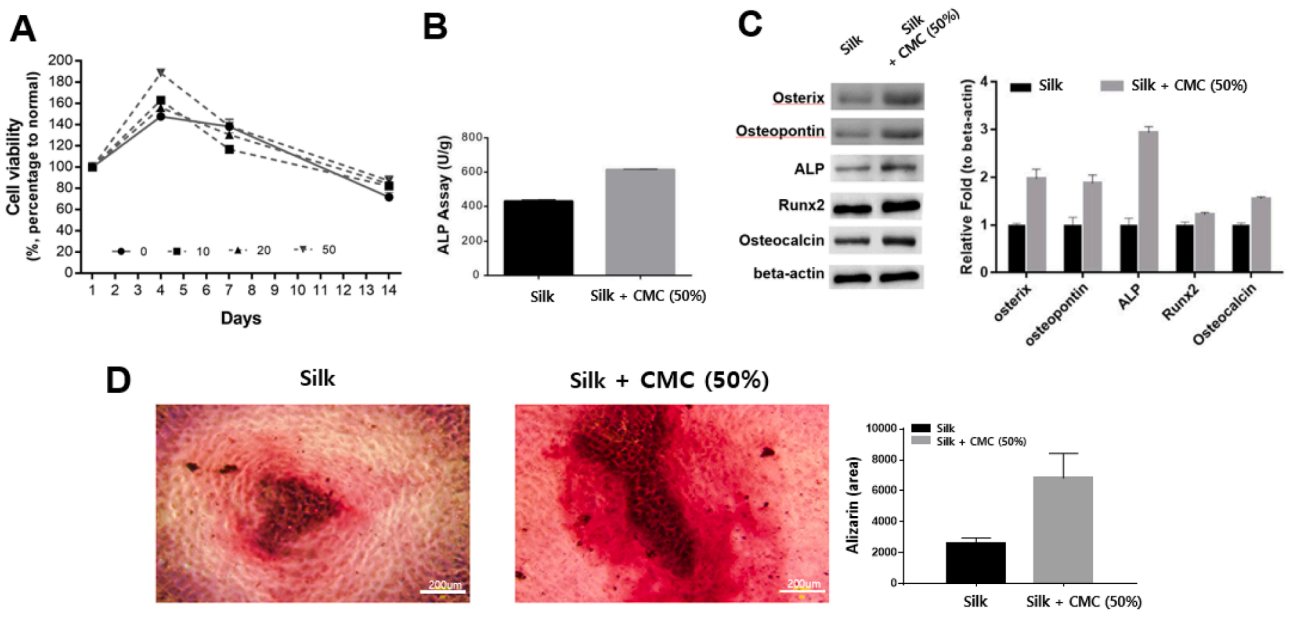

Fig. 5. The beneficial effect of CMC-containing scaffold on osteogenic differentiation. (A) The viability of bone marrow mesenchymal stem cells was measured by culturing the cells on Silks and Silks + CMC (50 %) composite scaffolds. Cell viability did not differ between Silks and Silks + CMC composite scaffolds. CMC concentrations of 10 mg/ml and 20 mg/ml were considered suitable for cell survival. (B) ALP activity was measured in each Silks and CMC added Silks scaffold. (C) Osteogenic differentiation of bone marrow mesenchymal stem cells was evaluated. In western blot analysis, bone-related protein expression amounts were evaluated by western blot analysis of bone marrow mesenchymal stem cells (left) and it is presented in the quantitative graph (right). (D) Bone nodule was stained with alizarin red S in two groups of Silks and Silks + CMC (50 %) composite scaffolds (left). The formed nodules were quantified by the stained area and optical density (right).

blotting. The protein levels of osteocytic markers, such as osterix, osteopontin, ALP, Runx2, and osteonectin showed a higher increase in the scaffold with a CMC concentration of 50 % than that in the scaffold with no CMC compared to the control group (Fig. 5C). To confirm the effect of each scaffold on osteocyte differentiation, Alizarin Red S was used. Calcium staining using Alizarin Red S was performed on day 14 in each silks or CMC-added silks sample to confirm forming bone nodule (Fig. 5D, left). The bone nodule was semi-quantified by the red stained area, and the area is shown in the graph (Fig. 5D, right). After 14 days of culture, it was confirmed that Silks + CMC (50 %) differentiated into osteocytes more than silks alone, and differentiation started after 2 weeks.

3.6. Fourier-Transform infrared (FTIR) spectroscopy analysis

FTIR analysis was performed to investigate the chemical interactions and structural characteristics of the Silks and Silks + CMC (50 %) composite scaffolds. Distinct peaks were observed in the silks-only scaffold at 1640 cm^{-1} and 1515 cm^{-1}, corresponding to the Amide I and Amide II bands, which indicate the presence of protein structures (Fig. 3D). These peaks are characteristic of the β-sheet conformation of silks, associated with the scaffold's mechanical stability and structural integrity. In contrast, the Silks CMC composite scaffold displayed an additional peak near 3400 cm^{-1}, attributed to the O—H stretching vibrations introduced by carboxymethyl cellulose (CMC), a known hydrophilic component. This peak suggests that CMC incorporation enhances the scaffold's hydrophilicity, potentially improving its ability to retain moisture and promote cell interaction. The observed shifts and intensities of the Amide I and II peaks were consistent across both scaffolds, indicating that the structural integrity of silks was maintained despite CMC addition. This FTIR analysis confirms the successful integration of CMC into the scaffold without disrupting the fundamental protein structure of silks.

3.7. Fluorescence-Activated cell sorting (FACS) analysis

FACS analysis was conducted to examine the expression of osteogenic markers CD73, CD90, and CD105 in treated cell populations, providing insight into osteogenesis. These markers are commonly associated with mesenchymal stem cells and osteogenic differentiation potential. The FACS results revealed significantly higher expression levels of CD73, CD90, and CD105 in the experimental group compared to controls (supplementary Figure 2), indicating enhanced osteogenic activity. In particular, the increased expression of CD105, a marker linked to vascular and osteogenic lineage commitment, suggested that the treatment protocol promotes differentiation towards an osteogenic phenotype. These findings support the hypothesis that the treatment enhances osteogenesis, as evidenced by the upregulation of key osteogenic markers. This FACS analysis thereby confirms the effectiveness of the scaffold in promoting osteogenic differentiation, consistent with the goals of bone tissue engineering.

4. Discussion

The macroscopic evaluation of the scaffolds demonstrated that the inclusion of CMC in the silks matrix led to an enhanced porous structure, with pore size increasing in tandem with the CMC concentration. This pore formation likely results from the interaction between CMC and silks during the freeze-drying process, where CMC contributes to a more hydrophilic and expansive network within the scaffold. The increased porosity and softer texture in the Silks-CMC composites align with previous studies indicating that higher CMC content can promote scaffold hydration and nutrient diffusion, which are crucial for cellular growth and differentiation. These macroscopic modifications, achieved by varying CMC concentrations, suggest that Silks/CMC scaffolds can be effectively tailored to create an optimal environment for osteogenic applications. Enhanced porosity, as seen in the silks -CMC composites, supports the hypothesis that such scaffolds could improve osteogenic outcomes by facilitating cell infiltration, nutrient exchange, and waste removal. In summary, the macroscopic evaluation confirms that the

CMC incorporation directly influences the scaffold's physical structure, creating an adaptable framework with potential advantages in bone tissue engineering applications.

The physical properties of the CMC and silks polymers were mechanically, chemically, and biologically analyzed in this study. The CMC-containing scaffold played an important role in facilitating osteogenic, ossification of BMSCs.

The solvent-casting freeze-drying method was effective for fabricating a porous scaffold containing silks, as the scaffold maintained its external shape and exhibited no defects, highlighting its structural integrity (Fig. 1). The SEM image of the prepared porous silks/CMC scaffold confirmed that the inner and side porous shapes were not different (Fig. 2). The similarity between the porous shapes of the support and salt particles suggests the successful replication of the desired morphology. Additionally, the lack of significant morphological differences indicates that the presence of silks had a minimal impact on the overall porous structure during the preparation process. These results demonstrate the successful fabrication of the porous scaffold and the suitability of silks as a component in its production and support the suitability of silks as a component in the fabrication of the porous scaffold. (Fig. 2).

In the H—NMR spectrum data, the change in the degree of substitution of the catechol group in silks/CMC corresponded to the amount of CMC in an aqueous solution at pH 5.5, as the degree of substitution increased with increasing amounts of CMC (Fig. 3B). However, at an input amount of 1 g or more, there was no significant change, but the degree of substitution of the catechol group changed when the pH increased from 5.5 to 7.5. Since silks have low solubility in water at neutral pH, the degree of substitution was lower at pH 6.5 than that observed at pH 5.5. However, at pH 7.5, the degree of substitution was slightly reduced owing to the low reactivity of the amine group of the silks, which was attributed to the partially oxidized CMC. Therefore, the amount of CMC (1 g) and pH (6.5) were fixed as the reaction conditions for silks /CMC, with a maximum degree of substitution of 38.6 % (Fig. 3B).

The dye did not penetrate the silks-only scaffold even after 20 min; however, it nearly completely penetrated the CMC-containing scaffold. In addition, the penetration rate increased as the CMC content increased. This increased hydrophilicity is attributed to the presence of carboxymethyl groups in CMC, which enhance its water-binding capacity. Additionally, the silks component, which is composed of hydrophilic amino acids, such as serine and glycine, contributes to the overall hydrophilicity of the scaffold.

With the addition of CMC, the expression of each bone-related protein in BMSCs was observed on day 6 of culture but was hardly expressed on day 3 (Fig. 4). In the MTT assay, the viability of BMSCs slightly increased (Fig. 5A). This is because, for cells to attach to a material, serum proteins must be absorbed onto the material. Because of its hydrophobic surface, CMC imparts hydrophilicity to the silks scaffold with no direct interaction between the cell and the material, thereby inducing serum protein adsorption. This effect is considered beneficial for cell viability. The positive effects on the growth and proliferation of these cells could be attributed to the biocompatibility and hydrophilicity of silks. This should be considered an important factor in the design of future Silks + CMC (50 %) composite scaffolds. Currently, we are studying the preparation of various carriers containing silks and the effects of silks on the ossification of BMSCs and expect their application in stem cell differentiation.

5. Conclusions

This study focused on the facilitating effect of the CMC-containing scaffold on bone differentiation. Improving binding efficiency in bone formation after implanted scaffold, CMC was added to silks. CMC-containing scaffolds were thermally stable, increased hydrophilicity and porosity of scaffolds, and additionally enhanced ALP activity. Differentiation of BMSCs into osteocytes was detected more in CMC-containing scaffolds than in silks-only scaffolds. Therefore, our results suggest that the CMC-containing scaffold could play an important role in ossification of BMSCs, which could serve as a potential application of such scaffolds in regenerative medicine.

Funding

This research did not receive any specific grant from funding agencies in the public, commercial, or not-for-profit sectors.

CRediT authorship contribution statement

Woong Jin Lee: Writing – original draft, Data curation, Conceptualization. **Kyoungjoo Cho:** Writing – original draft. **Dayoon Lee:** Writing – review & editing, Data curation. **Seungmin Lee:** Data curation. **Hyojae Jeon:** Writing – review & editing, Data curation. **Aaron Youngjae Kim:** Formal analysis. **Gyung Whan Kim:** Conceptualization.

Declaration of competing interest

The authors declare that they have no known competing financial interests or personal relationships that could have appeared to influence the work reported in this paper.

Supplementary materials

Supplementary material associated with this article can be found, in the online version, at doi:10.1016/j.bbiosy.2024.100103.

Data availability

Data will be made available on request.

References

[1] Bharathi R, Shree Ganesh S, Harini G, Kumari Vatsala R, Anushikaa R, Aravind S, Abinaya S, Selvamurugan N. Chitosan-based scaffolds as drug delivery systems in bone tissue engineering. Int J Biol Macromol 2022;222(Part A):132–53.
[2] Atwa A, Sofy MR, Fakhrelden SM, Darwish O, Mehany AB, Sofy AR, Bakry S. Biodegradable materials from natural origin for tissue engineering and stem cell technologies. In: Ali GAM, Makhlouf ASH, editors. Handbook of biodegradable materials. Springer; 2022. p. 1–16.
[3] Cañas-Gutiérrez A, Martinez-Correa E, Suárez-Avendaño D, Arboleda-Toro D, Castro-Herazo C. Influence of bacterial nanocellulose surface modification on calcium phosphates precipitation for bone tissue engineering. Cellulose 2020;27:10747–63.
[4] Filippi M, Gordian B, Chaaban M, Scherberich A. Natural polymeric scaffolds in bone regeneration. Front Bioeng Biotechnol 2020;8:474.
[5] Zuluaga-Vélez A, Quintero-Martinez A, Orozco LM, Sepúlveda-Arias JC. Silk fibroin nanocomposites as tissue engineering scaffolds – A systematic review. Biomedicine & Pharmacotherapy 2021;141:111924.
[6] Reizabal A, Costa CM, Pérez-Álvarez L, Vilas-Vilela JL, Lanceros-Méndez S. Silk fibroin as a sustainable advanced material: material properties and characteristics, processing, and applications. Adv Funct Mater 2023;33(3):2210764.
[7] Florczak A, Deptuch T, Kucharczyk K, Dams-Kozłowska H. Systemic and local silk-based drug delivery systems for cancer therapy. Cancers (Basel) 2021;13(21):5389.
[8] Yonesi M, Garcia-Nieto M, Guinea GV, Panetsos F, Pérez-Rigueiro J, González-Nieto D. Silk fibroin: an ancient material for repairing the injured nervous system. Pharmaceutics 2021;13(3):429.
[9] Zhang Q, Li M, Hu W, Wang X, Hu J. Silk-based biomaterials in tissue engineering: general approaches and potential stem cell therapies. Stem Cells Int 2021;2021:7141550.
[10] Amiryaghoubi N, Fathi M, Pesyan NN, Samiei M, Barar J, Omidi Y. Bioactive polymeric scaffolds for osteogenic repair and bone regenerative medicine. Med Res Rev 2020;40(5):1833–70.
[11] Branković M, Živić F, Grujović N, Stojadinović I, Milenković S, Kotorčević N. Review of spider silk applications in biomedical and tissue engineering. Biomimetics 2024;9(169).
[12] Janmohammadi M, Nazemi Z, Mahmoud Salehi AO, Seyfoori A, John JV, Nourbakhsh MS, Akbari M. Cellulose-based composite scaffolds for bone tissue engineering and localized drug delivery. Bioact Mater 2023;20:137–63.
[13] Kryuchkova A, Savin A, Kiseleva A, Dukhinova M, Krivoshapkina E, Krivoshapkin P. Magnetothermal spider silk-based scaffolds for cartilage regeneration. Int J Biol Macromol 2023;253(Part 6):127246.

[14] Nikam VS, Punde DS, Bhandari RS. Silk fibroin nanofibers enhance cell adhesion of blood-derived fibroblast-like cells: a potential application for wound healing. Indian J Pharmacol 2020;52(4):306.
[15] Eivazzadeh-Keihan R, Zare-Bakheir E, Aliabadi HAM, Gorab MG, Ghafuri H, Maleki A, Mahdavi M. A novel, bioactive and antibacterial scaffold based on functionalized graphene oxide with lignin, silk fibroin, and ZnO nanoparticles. Sci Rep 2022;12(1):8770.
[16] Arumugam M, Murugesan B, Pandiyan N, Chinnalagu DK, Rangasamy G, Mahalingam S. Electrospinning cellulose acetate/silk fibroin/Au-Ag hybrid composite nanofiber for enhanced biocidal activity against MCF-7 breast cancer cell. Mater Sci Eng: C 2021;123:112019.
[17] Francisco EM, Zoccolotti JdO, Tiomno Tiomnova O, Tolaba AG, Rodriguez Chanfrau JE, Jorge JH, Basmaji P, Guastaldi AC. Sterilization of scaffolds of calcium phosphates and bacterial cellulose for their use in tissue regeneration. Biointerface Res Appl Chem 2021;11(3):10089–98.
[18] Asensio Ruiz MA, Fuster MG, Martínez Martínez T, Montalbán MG, Cenis JL, Víllora G, Lozano-Pérez AA. The effect of sterilization on the characteristics of silk fibroin nanoparticles. Polymers (Basel) 2022;14(3):498.
[19] Rodriguez M, Kluge JA, Smoot D, Kluge MA, Schmidt DF, Paetsch CR, Kaplan DL. Fabricating mechanically improved silk-based vascular grafts by solution control of the gel-spinning process. Biomaterials 2020;230:119567.
[20] Panaitescu DM, Stoian S, Frone AN, Vlăsceanu GM, Baciu DD, Gabor AR, Nicolae CA, Radiţoiu V, Alexandrescu E, Căşărică A, Damian C, Stanescu P. Nanofibrous scaffolds based on bacterial cellulose crosslinked with oxidized sucrose. Int J Biol Macromol 2022;221:381–97.
[21] Kamalvand M, Biazar E, Daliri-Joupari M, Montazer F, Rezaei-Tavirani M, Heidari-Keshel S. Design of a decellularized fish skin as a biological scaffold for skin tissue regeneration. Tissue Cell 2021;71:101509.
[22] Asadpour S, Kargozar S, Moradi L, Ai A, Nosrati H, Ai J. Natural biomacromolecule based composite scaffolds from silk fibroin, gelatin and chitosan toward tissue engineering applications. Int J Biol Macromol 2020;154:1285–94.
[23] Shi Y, Kang X, Wang Y, Bian X, He G, Zhou M, Tang K. Exosomes derived from bone marrow stromal cells (BMSCs) enhance tendon-bone healing by regulating macrophage polarization. Med Sci Mon: Int Med J Exp Clin Res 2020;26.
[24] Liu A, Lin D, Zhao H, Chen L, Cai B, Lin K, Shen SG. Optimized BMSC-derived osteoinductive exosomes immobilized in hierarchical scaffold via lyophilization for bone repair through Bmpr2/Acvr2b competitive receptor-activated Smad pathway. Biomaterials 2021;272:120718.
[25] Lei L, Hu Y, Shi H, Bao Z, Wu Y, Jiang J, Li X. Biofunctional peptide-click PEG-based hydrogels as 3D cell scaffolds for corneal epithelial regeneration. J Mater Chem B 2022;10(31):5938–45.
[26] Trivedi S, Srivastava K, Gupta A, Saluja TS, Kumar S, Mehrotra D, Singh SK. A quantitative method to determine osteogenic differentiation aptness of scaffold. J Oral Biol Craniofac Res 2020;10(2):158–60.
[27] Zakhireh S, Adibkia K, Beygi-Khosrowshahi Y, Barzegar-Jalali M. Osteogenesis promotion of selenium-doped hydroxyapatite for application as bone scaffold. Biol Trace Elem Res 2021;199:1802–11.
[28] Biranje SS, Sun J, Cheng L, Cheng Y, Shi Y, Yu S, Liu J. Development of cellulose nanofibril/casein-based 3D composite hemostasis scaffold for potential wound-healing application. ACS Appl Mater Interfaces 2022;14(3):3792–808.
[29] Wang X, Guo C, Guo L, Wang M, Liu M, Song Y, Kaplan DL. Radially aligned porous silk fibroin scaffolds as functional templates for engineering human biomimetic hepatic lobules. ACS Appl Mater Interfaces 2021;14(1):201–13.
[30] Karavasili C, Fatouros DG. Self-assembling peptides as vectors for local drug delivery and tissue engineering applications. Adv Drug Deliv Rev 2021;174:387–405.
[31] Rasouli M, Naghib SM. Mechanism of inhibition of hydroxyapatite nanoparticles on cancer cells and recent advances in the field. Curr Mech Adv Mater 2021.